Cancer Research

Tumor-Associated Macrophages Enhance Tumor Hypoxia and Aerobic Glycolysis

Hoibin Jeong[1], Sehui Kim[2], Beom-Ju Hong[1], Chan-Ju Lee[1], Young-Eun Kim[1], Seoyeon Bok[1], Jung-Min Oh[1], Seung-Hee Gwak[1], Min Young Yoo[3], Min Sun Lee[3], Seock-Jin Chung[3], Joan Defrêne[4], Philippe Tessier[4], Martin Pelletier[4], Hyeongrin Jeon[5], Tae-Young Roh[1,5], Bumju Kim[6], Ki Hean Kim[6], Ji Hyeon Ju[7], Sungjee Kim[8], Yoon-Jin Lee[9], Dong-Wan Kim[10], Il Han Kim[11,12,13], Hak Jae Kim[11,12,13], Jong-Wan Park[14], Yun-Sang Lee[3], Jae Sung Lee[3], Gi Jeong Cheon[3,12,13], Irving L. Weissman[15], Doo Hyun Chung[2], Yoon Kyung Jeon[2], and G-One Ahn[1,5]

Abstract

Tumor hypoxia and aerobic glycolysis are well-known resistance factors for anticancer therapies. Here, we demonstrate that tumor-associated macrophages (TAM) enhance tumor hypoxia and aerobic glycolysis in mice subcutaneous tumors and in patients with non–small cell lung cancer (NSCLC). We found a strong correlation between CD68 TAM immunostaining and PET ^{18}fluoro-deoxyglucose (FDG) uptake in 98 matched tumors of patients with NSCLC. We also observed a significant correlation between *CD68* and glycolytic gene signatures in 513 patients with NSCLC from The Cancer Genome Atlas database. TAM secreted TNFα to promote tumor cell glycolysis, whereas increased AMP-activated protein kinase and peroxisome proliferator-activated receptor gamma coactivator 1-alpha in TAM facilitated tumor hypoxia. Depletion of TAM by clodronate was sufficient to abrogate aerobic glycolysis and tumor hypoxia, thereby improving tumor response to anticancer therapies. TAM depletion led to a significant increase in programmed death-ligand 1 (PD-L1) expression in aerobic cancer cells as well as T-cell infiltration in tumors, resulting in antitumor efficacy by PD-L1 antibodies, which were otherwise completely ineffective. These data suggest that TAM can significantly alter tumor metabolism, further complicating tumor response to anticancer therapies, including immunotherapy.

Significance: These findings show that tumor-associated macrophages can significantly modulate tumor metabolism, hindering the efficacy of anticancer therapies, including anti-PD-L1 immunotherapy.

[1]Division of Integrative Biosciences and Biotechnology, Pohang University of Science and Technology (POSTECH), Pohang, Gyeongbuk, Korea. [2]Department of Pathology, Seoul National University College of Medicine, Seoul, Korea. [3]Department of Nuclear Medicine, Seoul National University College of Medicine, Seoul, Korea. [4]Department of Microbiology-Infectious Diseases and Immunology, Faculty of Medicine, Laval University, Ville de Québec, Québec, Canada. [5]Department of Life Sciences, POSTECH, Pohang, Gyeongbuk, Korea. [6]Department of Mechanical Engineering, POSTECH, Pohang, Gyeongbuk, Korea. [7]Division of Rheumatology, Department of Internal Medicine, Seoul St. Mary's Hospital, Seoul, Korea. [8]Department of Chemistry, POSTECH, Pohang, Gyeongbuk, Korea. [9]Division of Radiation Biomedical Research, Korea Institute of Radiological and Medical Sciences, Seoul, Republic of Korea. [10]Department of Internal Medicine, Seoul National University College of Medicine, Seoul, Korea. [11]Department of Radiation Oncology, Seoul National University College of Medicine, Seoul, Korea. [12]Cancer Research Institute, Seoul National University College of Medicine, Seoul, Korea. [13]Institute of Radiation Medicine, Seoul National University College of Medicine, Seoul, Korea. [14]Department of Pharmacology, Seoul National University College of Medicine, Seoul, Korea. [15]Stem Cell Biology and Regenerative Medicine, Stanford University, Stanford, California.

Note: Supplementary data for this article are available at Cancer Research Online (http://cancerres.aacrjournals.org/).

H. Jeong and S. Kim contributed equally to this article.

Corresponding Authors: G-One Ahn, Pohang University of Science and Technology, 77 CheongAm-Ro, Nam-Gu, Pohang, Gyeongbuk 37673, Korea. Phone: 821092123870; Fax: 82542798379; E-mail: goneahn@gmail.com; and Yoon Kyung Jeon, Seoul National University College of Medicine, 103 Daehak-Ro, Jongno-Gu, Seoul 03080, Korea. Phone: 8227408323; Fax: 8227435530; E-mail: ykjeon@snu.ac.kr

doi: 10.1158/0008-5472.CAN-18-2545

©2019 American Association for Cancer Research.

Introduction

Tumor hypoxia and glycolysis have long been recognized as major resistance factors contributing to failures of chemo- and radiotherapy (1, 2). Traditionally, tumor hypoxia is known to occur by two mechanisms: chronic or acute hypoxia (2). Chronic hypoxia occurs as a result of rapid proliferation of cancer cells and hence being constantly forced away from blood vessels beyond the oxygen diffusion distance of approximately 150 μm (2). Acute hypoxia on the other hand occurs by a temporary cessation of the blood flow due to highly disorganized tumor vasculature (2). Regardless of the mechanism, tumor hypoxia has been extensively documented for their contribution to resistance to all anticancer therapies including chemotherapy (2), surgery (3), radiotherapy (2), and recently immunotherapy (4).

Aerobic glycolysis, also known as Warburg effect, is a phenomenon whereby many types of tumors exhibit a preference of glucose over the oxygen for their energy substrate (5), and this has allowed us to track solid tumors in patients with PET using ^{18}fluoro-deoxyglucose (FDG) radioactive tracer (6). Although several mechanisms for Warburg effect have been suggested including mitochondrial defects, adaptation to hypoxia [hence activation of hypoxia-inducible factor (HIF)], and oncogenic signals such as *MYC* and *RAS* (7), the exact mechanism is still controversial. Tumor glycolysis has also been reported to influence the therapy outcome (8). Preclinical studies have suggested that glycolysis can increase DNA repair enzyme expressions including Rad51 and Ku70, which can facilitate radiation-induced DNA double-strand break repair (9). Lactate, a major byproduct of glycolysis, has recently been shown to be

Downloaded from http://aacrjournals.org/cancerres/article-pdf/79/4/795/2786616/795.pdf by guest on 15 September 2022

utilized as a fuel source for oxidative phosphorylation in nearby cancer cells (10), which can promote the tumor recurrence following anticancer therapies.

Tumor-associated macrophages (TAM) are bone marrow–derived immune cells recruited to tumors and have been extensively reported for their protumoral role (11). Recruited to tumors by various tumor-secreting factors including stromal cell–derived factor-1 (SDF1; ref. 12), VEGF (13), semaphorin 3A (14), and colony-stimulating growth factor-1 (CSF1; ref. 15), TAMs have been shown to produce various growth factors and proteases necessary for tumor survival (11) or immunosuppressive cytokines inhibiting antitumor immune responses (16). Macrophages in general are known to be polarized to either classically activated M1 macrophages or alternatively activated M2 phenotype depending on the cytokine milieu in which they are exposed (17). Bacterial-derived products such as lipopolysaccharide have been shown to polarize macrophages toward M1 phenotype (17), while parasite-associated signals such as IL4 and IL13 can lead to M2-polarized macrophages with increased tissue repair abilities (17). It has been suggested that TAMs are M2-like, although various subpopulations of TAM have been also identified including TIE2-positive macrophages (18), programmed cell death protein-1 (PD-1)–expressing TAM (19), and C-C chemokine receptor type-2 (CCR2)–expressing TAM (20).

In this study, we demonstrate clinically and preclinically that TAMs are a novel contributor to tumor hypoxia and aerobic glycolysis by competing oxygen and glucose with cancer cells. We further observed that TAM can significantly interfere with T-cell infiltration thereby masking programmed death-ligand 1 (PD-L1) expression in the tumors. We believe that our results have an important clinical implication such that patients with high infiltration of TAM in their tumors may poorly respond to all anticancer therapies, including the latest immunotherapy.

Materials and Methods

CD68 immunostaining and PET index analysis in patients with non–small cell lung cancer

Immunohistochemistry for TAM was performed in 98 patients with non–small cell lung cancer (NSCLC) biopsy samples collected at Seoul National University Hospital (SNUH) by using CD68 antibodies (PG-M1; DakoCytomation) with Bond-Max autostainer. The slides were scanned by virtual microscopy (Aperio Technologies). For enumeration of immune cells, ten different fields per tumor were captured from virtual microscopic images (an area of 1 mm^2). The average number of $CD68^+$ TAM per unit area (mm^2) was then counted manually. Median values of the numbers in CD68-positive TAM were used as a cutoff to divide $CD68^{low}$ versus $CD68^{Hi}$ tumors. This study followed the World Medical Association Declaration of Helsinki recommendations and was approved by the Institutional Review Board (IRB) of SNUH (IRB No. 1404-100-572). Informed consent for participation in the study was waived by the IRB of SNUH on the basis that this study was a retrospective study using archived material and did not pose increased risk to the patients.

The Cancer Genome Atlas analysis

Genomic analyses were performed to examine the correlation between CD68 (*CD68*), TNFα (*TNF*), HIF1α (*HIF1A*), and glycolysis-related molecules, including glucose transporter 1 [GLUT1 (*solute carrier family 2 member, SLC2A1*)] and hexokinase 2 [HK2 (*HK2*)]. The level 3 data of The Cancer Genome Atlas (TCGA), which were downloaded from the UCSC Cancer Browser (https://genome-cancer.ucsc.edu) on June 3, 2015, were used for analysis. We used mRNA expression data of the Lung Adenocarcinoma dataset, which included 513 tumor samples. mRNA expression data generated using the Illumina HiSeq V2 platform were presented as reads per kilobase per million and transformed into log 2 values for analysis. All statistical analyses were performed using SPSS software (version 21; IBM Corp.), and images were created by the GraphPad Prism 5 software. For TCGA data, the statistical significance of two continuous variables, such as mRNA level of CD68 (*CD68*), TNFα (*TNF*), HIF1α (*HIF1A*), GLUT1 (*SLC2A1*), and HK2 (*HK2*), was calculated by Pearson and Spearman correlation analysis. Two-sided P values <0.05 were considered statistically significant.

Mice and *in vivo* experiments

Four- to six-week-old C57BL/6 or BALB/c-nude female mice (OrientBio Inc.) were maintained in germ-free environment and had access to food and water *ad libitum*. All animal procedures were approved by Institutional Animal Care and Use Committee at POSTECH. Lewis lung carcinoma (LLC; provided by Dr. J. Martin Brown, Stanford University, Stanford, CA) cells were routinely maintained (up to 20 passages) in DMEM (Welgene) supplemented with 10% FBS (Omega Scientific, Inc.). Metformin (Sigma-Aldrich), oligomycin (Sigma-Aldrich), or 2-deoxyglucose (2-DG; Sigma-Aldrich) was injected to tumor-bearing mice at 25 mg/kg (at every 12 hours), 0.5 mg/kg (at everyday), or 500 mg/kg (at every 48 hours), respectively. Purified anti-mouse CD8α antibody clone 53-6.7 (BioLegend) was injected intraperitoneally at 150 μg at 48 hours before tumor harvest. PD-L1 Ab clone 10F.9G2 or control IgG (BioXCell) was injected intraperitoneally at 100 μg every other day. Clodronate or vehicle liposome (Encapsula Nano Science) was injected intravenously twice at 24-hour interval, 24 hours prior to the tumor harvest. For combination with metformin, 2-DG, oligomycin, or PD-L1 Ab, clodronate or vehicle liposome was intravenously injected every second day. To detect tumor hypoxia, pimonidazole (Hypoxyprobe-1; HPI Inc.) was intraperitoneally injected at 60 mg/kg at 1 hour prior to the tumor harvest. Hoechst 33342 (Sigma-Aldrich) was administered intravenously at 50 mg/kg at 20 minutes before sacrificing mice.

In vitro experiments

LLC cells expressing 5 × HRE-GFP were generated by transfecting 5 × HRE-GFP plasmid (provided from Dr. J. Martin Brown in Stanford University) using TransIT-X2 (Mirus) according to the manufacturer's protocol. After 48 hours, stably transfected cells were selected by G418 (A. G. Scientific, Inc.) at 1 mg/mL over 2 weeks. HRE-GFP expression in stably transfected cells was confirmed by monitoring GFP signals from cells treated with 400 μmol/L of CoCl2 for 24 hours under a fluorescent microscope (EVOS Cell Imaging Systems; Thermo Fisher Scientific) or by FACS using cells that had been incubated in a hypoxic chamber (BACTRON Anaerobic Chamber; Shel Lab) for up to 48 hours. Bone marrow–derived macrophages (BMDM) were prepared as described previously (21). Murine recombinant proteins TNFα, IFNγ, CXCL1, CXCL2, IL1β, IL6, and IL10 were all purchased from Peprotech and for glucose uptake experiment they were treated at the following concentrations with low glucose-supplemented medium for 24 hours:

Downloaded from http://aacrjournals.org/cancerres/article-pdf/79/4/795/2786616/795.pdf by guest on 15 September 2022

TNFα at 20 ng/mL, IFNγ at 80 ng/mL, CXCL1 at 100 ng/mL, CXCL2 at 100 ng/mL, IL1β at 50 ng/mL, IL6 at 20 ng/mL, or IL10 at 10 ng/mL. BMDM were treated with AICAR (Tocris) at 1 mmol/L prepared in culture medium supplemented with 1% serum for 2 hours. For Western blot analyses, BMDM were treated with 10 mmol/L metformin in low glucose media for 2 hours. For *in vitro* coculture system, lower compartment of a 12-well plate was seeded with either LLC or BMDM at 4×10^5 cells per well density. After 12 hours, medium was replaced by low glucose medium, and a transwell insert (modified Boyden chamber with 0.4 μm pore size; Corning) containing BMDM or LLC at 4×10^5 cells was placed and further incubated for 24 hours. For glucose add back experiment, glucose was added to the lower compartment of the Boyden chamber, which was originally low glucose medium (1 g/L; Thermo Fisher Scientific) so that the final concentration of the glucose after adding back becomes 4.5 g/L, which was equivalent to commercially available high glucose medium (Welgene). For LLC; HRE-GFP and BMDM coculture experiment, BMDM at 5×10^5 cells were seeded directly onto a 6-well plate in 1% serum-supplemented media for 12 hours after LLC; HRE-GFP at 5×10^5 cells had been plated. After 24-hour further incubation, cells were harvested and GFP signals from LLC; HRE-GFP were detected by FACS after negative selection using CD11b and F4/80 markers to exclude BMDM.

FACS analysis

LLC tumors were harvested when the tumor size reached approximately 150 mm^3, followed by enzyme digestion using a cocktail consisting of collagenase (Worthington), pronase (Calbiochem), and DNase I (Sigma-Aldrich). Tumors prepared in single-cell suspensions were then filtered through 100 μm Cell Strainer (Corning) and further incubated in 1 × BD Pharm Lyse (BD Biosciences) in PBS for 10 minutes on ice. Cells were then washed in FACS buffer (Ca^{2+}-free PBS containing 3% FBS) and following antibodies were added: PE-Cy7 anti-CD11b (eBioscience), APC anti-F4/80 (eBioscience), Keratin 4.62 antibody (Sigma-Aldrich), anti-pimonidazole (PAb2627AP; HPI Inc.), FITC anti-CD45 (BioLegend), PE-Cy7 anti-CD4 (BioLegend), Pacific Blue anti-CD8α (BioLegend), PE-Cy7 anti-CD8α (BioLegend), APC anti-CD44 (eBioscience), PerCP-Cy5.5 anti-CD62L (BioLegend), PE anti-IFNγ (eBioscience), or Pacific Blue anti-Granzyme B (BioLegend) antibodies. Secondary antibodies were anti-mouse Alexa 488 antibodies (Life Technologies) or anti-rabbit Alexa 488 (Life Technologies). For aerobic versus hypoxic tumor cell quantification, $Hoechst^{bright}Keratin^{+}$ cells were regarded as aerobic cells, whereas $Hoechst^{dim}Keratin^{+}$ cells or $pimonidazole^{+}$ cells were quantified as hypoxic cells where appropriate. $Hoechst^{bright}Keratin^{+}$ aerobic cancer cells were sorted freshly every time from a different batch of tumor-bearing animals in order to perform any individual functional/biochemical assay. For T-cell stimulation to quantify granzyme B (GzmB) and IFNγ, tumor cells made in single-cell suspension were incubated with eBioscience Cell Stimulation Cocktail containing protein transport inhibitors (Invitrogen) for 4 hours before antibody staining. For function analysis of mitochondria in BMDM, 5×10^5 cells in prewarmed PBS were stained with 500 nmol/L Mitotracker (Thermo Fisher Scientific) or 200 nmol/L tetramethylrhodamine, ethyl ester (TMRE; Abcam) for 30 minutes. After washing, samples were introduced to MoFlo XPD (Beckman Coulter) for sorting or LSR Fortessa 5 cell analyzer (BD Biosciences) for analysis.

Statistical analysis

Statistical comparisons of the data sets were performed by two-tailed Student *t* test, one-way ANOVA with Tukey post test, or two-way ANOVA with Bonferroni correction using Prism software (Version 4.00; GraphPad Inc.). Data were considered statistically significant when $P < 0.05$.

Additional information is available in Supplementary Methods.

Results

Clinical correlation between TAM infiltration and glycolysis in patients with NSCLC

To investigate whether TAMs play a role in tumor glycolysis, we first examined TAM in 98 biopsy samples taken from patients with stage I and II NSCLC (48 adenocarcinomas and 50 squamous cell carcinomas) whom had also been imaged for FDG PET by immunostaining for TAM using CD68 antibodies. We observed that there was a significant correlation between FDG uptake and TAM counts in tumors (Fig. 1A and B), as measured both by FDG maximal standardized uptake value (SUV_{max}; Fig. 1B) and 40% total lesion glycolysis (Fig. 1B). Reciprocal analyses by categorizing tumors into $CD68^{low}$ versus $CD68^{Hi}$ also revealed a significant difference in FDG SUV_{max} (Fig. 1C). Further examination into subgroup analyses revealed that the significance correlation between FDG uptake and TAM infiltration existed in adenocarcinomas but not in squamous cell carcinomas (Fig. 1D), perhaps due to the distinctly higher glucose uptake and glycolysis in squamous cell carcinomas, as reported recently (22). By analyzing TCGA database in 513 patients with adenocarcinoma NSCLC, we also found a strong correlation between *CD68* and glycolysis signatures, including *SLC2A1*, also known as GLUT1, (Fig. 1E) and *HK2* (Fig. 1E).

TAMs make tumors more glycolytic

To determine the molecular mechanism, we implanted LLC subcutaneously in mice and depleted TAM by intravenously administering clodronate liposome (Clod; Supplementary Fig. S1A), a liposomal preparation of bisphosphonate causing apoptosis selectively in macrophages (23). We first validated our clinical findings in a preclinical model by measuring FDG uptake in LLC tumors by PET (Fig. 2A) and found that Clod significantly lowered FDG signals (Fig. 2A and B). Moreover, we observed that ferumoxytol uptake, previously reported as an magnetic resonance (MR) contrast agent for TAM (24), was significantly reduced by Clod (Fig. 2A) and that this ferumoxytol uptake was colocalized with CD68-positive areas in tumors by IHC staining (Supplementary Fig. S1B). We then wished to examine genetic and functional changes of glycolysis in LLC modulated by TAM. To do this, we perfused the tumors with Hoechst 33342, a vascular perfusion dye, and sorted aerobic cells by FACS according to the brightness of Hoechst 33342 dye (25) in conjunction with Keratin-19 antibodies to label cancer cells (Supplementary Fig. S1C). By performing qRT-PCR, we observed that aerobic cancer cells ($Hoechst^{bright}Keratin^{+}$; Fig. 2C) depleted for TAM exhibited a significantly decreased gene expression in glycolytic pathways including *Slc2a1* (also known as *Glut1*), *pyruvate dehydrogenase kinase-1* (*Pdk1*), *pyruvate dehydrogenase* (*Pdh*), *phosphoglycerate kinase* (*Pgk*), *Hk2*, *glucose-6-phosphate dehydrogenase* (*G6pd*) as well as those in HIF signaling such as *Vegfa*, *carbonic anhydrase 9* (*Ca-9*), and *nitric oxide synthase-2* (*Nos2*; Fig. 2D).

Downloaded from http://aacrjournals.org/cancerres/article-pdf/79/4/795/2786616/795.pdf by guest on 15 September 2022

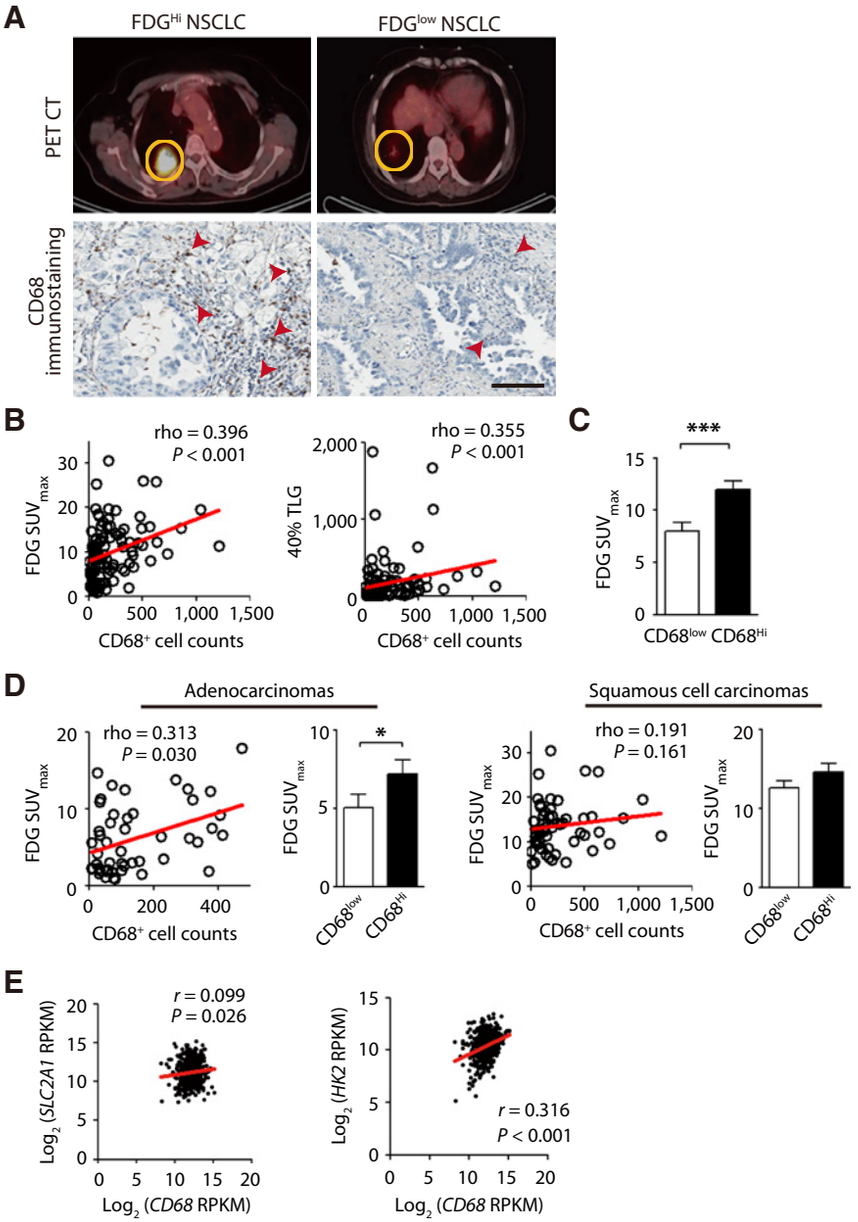

Figure 1.

Strong correlations between TAM infiltration and glycolysis in patients with NSCLC. **A,** Representative PET/CT images for FDG uptake (top) and immunostaining of CD68 (bottom) from paired tumors of patients with NSCLC. Top, yellow circles, location of tumors. Bottom, red arrowheads, CD68-positive TAM. Scale bar, 100 μm. **B,** Correlation between glycolysis and CD68-positive TAM in 98 patients with NSCLC paired results as in **A**. Glycolysis was analyzed as FDG maximal standardized uptake value (FDG SUV_{max}; left) or 40% total lesion glycolysis (TLG; right). **C,** FDG SUV_{max} values for $CD68^{low}$ ($n = 49$) or $CD68^{Hi}$ ($n = 49$) NSCLC tumors. **D,** Subgroup analyses of FDG uptake in adenocarcinomas ($n = 48$; left) or squamous cell carcinomas ($n = 50$; right) of NSCLC. *, $P < 0.05$; ***, $P < 0.001$ in **C** and **D** as determined by the Student *t* test. Data are the mean ± SEM. **E,** TCGA analysis between *CD68* and *SLC2A1* (left) or *HK2* (right) in 513 patients with adenocarcinoma NSCLC. *P* values are indicated in each plot.

There was no significant change in DNA repair gene such as *Parp1*, whereas *C-X-C motif chemokine ligand-12* (*Cxcl12*), a well-known HIF1-downstream target gene (26), was significantly increased in aerobic cancer cells depleted for TAM (Fig. 2D). To determine whether the gene expression changes would also reflect functional changes, we measured glucose uptake using ^{14}C-deoxyglucose as well as lactate production in the sorted cells. We observed that aerobic cancer cells depleted for TAM as above not only took up less glucose (Fig. 2E) but also produced a significantly reduced amount of lactate (Fig. 2E) and decreased GLUT1 protein expression (Fig. 2F). Furthermore, aerobic cancer cells depleted for TAM exhibited faster oxygen consumption kinetics (Fig. 2G), although mitochondrial potential (Supplementary Fig. S1D) or the total mitochondrial mass (Supplementary Fig. S1E) was not changed. These results thus indicate that depletion of TAM could switch the tumor metabolism from aerobic glycolysis to oxidative phosphorylation (OXPHOS). To prove this hypothesis, we sought to inhibit OXPHOS by administering metformin (27) or glycolysis by administering 2-DG (28) in LLC tumor–bearing mice that had been depleted for TAM with Clod. We found that the tumor growth inhibition was the most significant when depleted for TAM in combination with metformin (Fig. 2H) but not with 2-DG (Fig. 2I). Consistent with this result, we observed that oligomycin, another OXPHOS inhibitor (29), also resulted in a significant tumor growth inhibition (Supplementary Fig. S2A). Collectively, these results together suggest that TAM can significantly alter the tumor metabolism.

Downloaded from http://aacrjournals.org/cancerres/article-pdf/79/4/795/2786616/795.pdf by guest on 15 September 2022

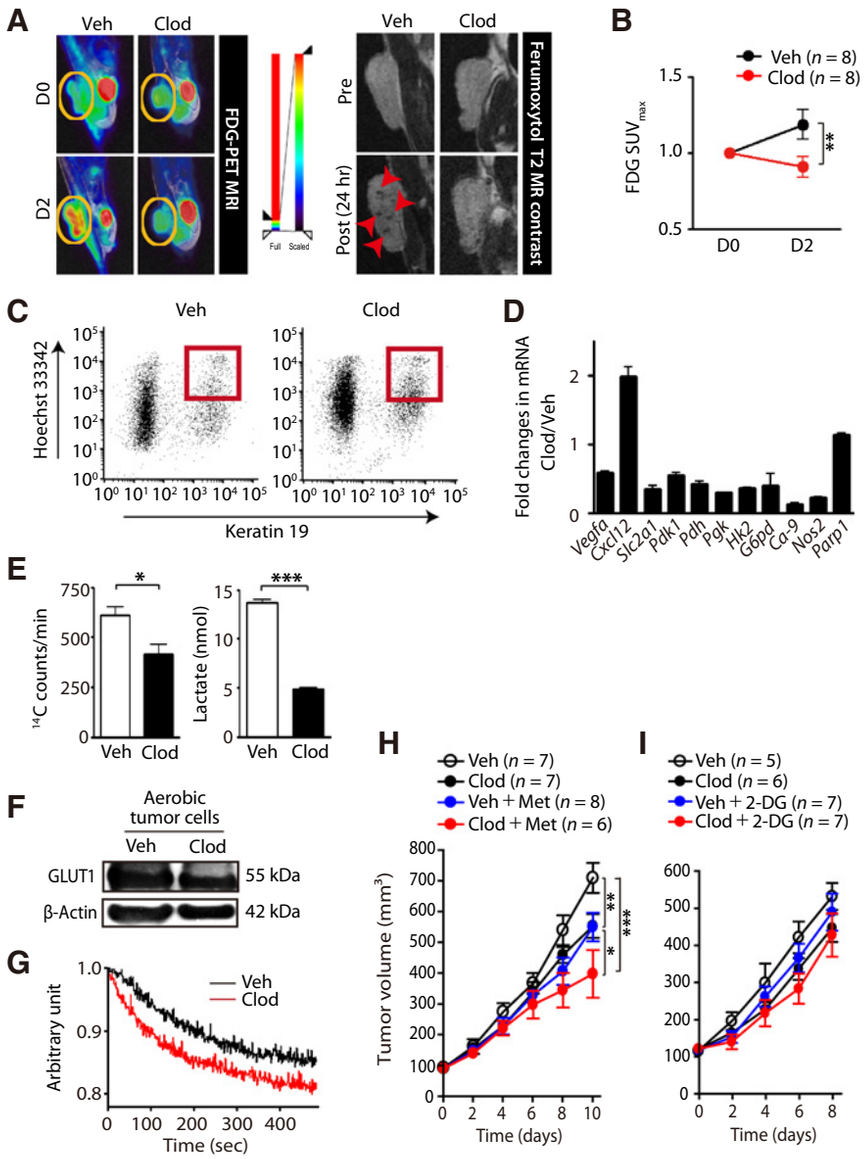

Figure 2.

TAMs make tumors more glycolytic. **A,** Left, PET/MRI images for FDG uptake in LLC tumors in mice before (D0, top) and after (D2, bottom) Veh or Clod treatment. Yellow circles, tumors. Right, T2-weighted MR images of LLC tumors treated with Veh or Clod pre (top)- or post (bottom)- contrast. Red arrowheads in Veh tumor, ferumoxytol-labeled TAM. **B,** FDG uptake SUV_{max} in **A**. **, $P < 0.01$, determined by two-way ANOVA. **C,** FACS plot indicating Hoechst^{bright}Keratin^{+} (red boxes) population of cells sorted as aerobic cancer cells. **D,** Fold changes in gene expression in FACS-sorted aerobic cancer cells from LLC tumors treated with Clod or Veh. **E,** Glucose uptake (left) and lactate production (right) from the sorted aerobic cancer cells as in **C**. Data in **D** and **E** are the mean ± SEM from at least triplicate samples. *, $P < 0.05$; ***, $P < 0.001$ by the Student *t* test. **F,** Western blot of FACS-sorted aerobic cancer cells in **C** for GLUT1. β-Actin was used as the loading control. **G,** Oxygen consumption kinetics in FACS-sorted aerobic cancer cells as described in **C**. **H,** LLC tumor growth in mice treated with Veh, Clod, Veh + metformin (Veh + Met), or Clod + metformin (Clod + Met). *, $P < 0.05$; **, $P < 0.01$; ***, $P < 0.001$, determined by two-way ANOVA. **I,** LLC tumor growth in mice treated with Veh, Clod, Veh + 2-DG, or Clod + 2-DG. Data in **H** and **I** are the mean ± SEM, with number of animals indicated in the graphs.

TAMs secrete TNFα to promote tumor glycolysis

We next sought what molecule(s) would be secreted from TAM to facilitate glycolysis in cancer cells. To do this, we set up a modified Boyden chamber coculturing LLC cancer cells and BMDM and examined gene expression changes in LLC cancer cells. We found that LLC cocultured with BMDM exhibited a significantly increased gene expression in many glycolytic genes including *Slc2a1*, *Pdk1*, *Pgk*, *Hk2*, and *lactate dehydrogenase A* (*Ldha*; Fig. 3A), although *Pdh* and *G6pd* did not exhibit such an increase (Fig. 3A). Moreover, LLC cocultured with BMDM took up more glucose (Fig. 3B) and produced more lactate (Fig. 3B) compared with LLC cultured alone, suggesting that this system well reflects tumors *in vivo*. Importantly, when we introduced glucose back to the LLC compartment of the coculture system with BMDM, glucose uptake to LLC returned to the basal level of LLC cultured alone (Fig. 3C), indicating that it was indeed glucose competition between cancer cells and macrophages. To identify TAM-secreted factor(s), we harvested supernatant from the coculture systems and exposed them to antibody array or luminex-based cytokine array. We observed that TNFα was significantly increased from both antibody array (Fig. 3D; Supplementary Fig. S2B) and luminex-based cytokine array (Fig. 3E), although there were several other cytokines including ILβ, CXCL1, CXCL2, IL10, and IL6 whose expression was upregulated in BMDM cocultured with LLC compared with BMDM alone (Fig. 3D; Supplementary Fig. S2B and S2C). To investigate which cytokines facilitate glucose uptake in LLC, we treated the above cytokines individually to LLC and found that glucose uptake was significantly increased when the cells were treated with TNFα (Fig. 3F; Supplementary Fig. S2E and S2F), but not with IL1β, CXCL1, nor CXCL2, the cytokines observed to be increased in cytokine array (Fig. 3D; Supplementary Fig. S2E) or with IL10 nor IL6 from luminex-based cytokine array (Supplementary Fig. S2C and S2F). Treatment of TNFα to

Downloaded from http://aacrjournals.org/cancerres/article-pdf/79/4/795/2786616/795.pdf by guest on 15 September 2022

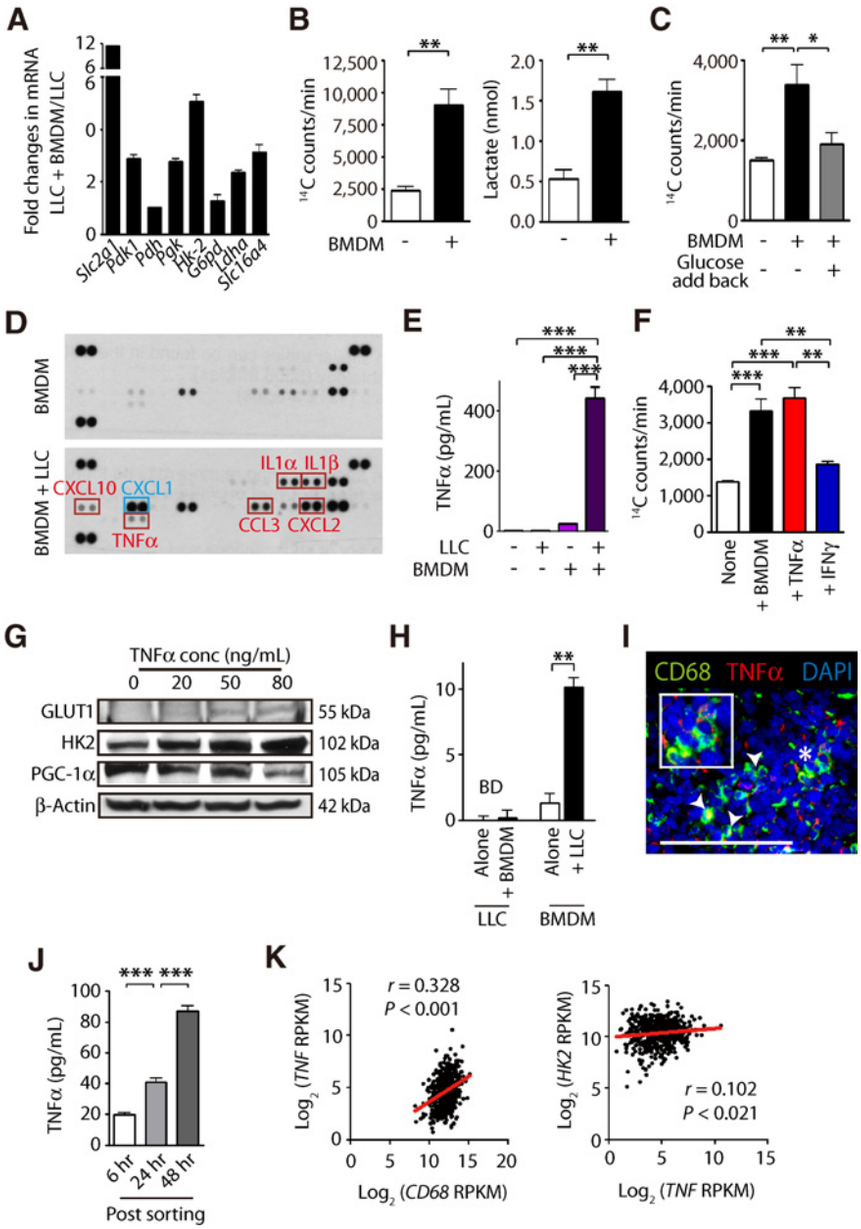

Figure 3.

Macrophages secrete TNFα to facilitate glycolysis in cancer cells. **A,** Gene expression changes in LLC cocultured with (LLC+BMDM) or without (LLC) BMDM. Data are the mean ± SEM from at least triplicate determinations. **B,** Glucose uptake (left) and lactate production (right) in LLC cocultured with or without BMDM. Data are the mean ± SEM for triplicate samples per group. **, $P < 0.01$ by Student *t* test. **C,** Glucose uptake in LLC cultured alone, cocultured with BMDM, or cocultured with BMDM with glucose added back to the LLC compartment of the coculture system. Data are the mean ± SEM for $n = 4$ replicates per group. *, $P < 0.05$; **, $P < 0.01$ by one-way ANOVA. **D,** Antibody cytokine arrays in the supernatant obtained from BMDM culture with (BMDM+LLC) or without (BMDM) LLC. Red boxes indicate those cytokines whose expressions were increased in BMDM cocultured with LLC compared with BMDM alone. Blue box, CXCL1, a cytokine produced by LLC cancer cells themselves (Supplementary Fig. S2D). **E,** Luminex cytokine assays for TNFα in the supernatant from culture media, LLC alone, BMDM alone, or BMDM cocultured with LLC. Data are the mean ± SEM for $n = 3$ replicates per group. ***, $P < 0.001$ by one-way ANOVA. **F,** Glucose uptake in LLC alone (none), LLC cocultured with BMDM (+BMDM), or LLC treated with TNFα (+TNFα) or with IFNγ (+IFNγ). Data are the mean ± SEM from $n = 3$ samples per group. **, $P < 0.01$; ***, $P < 0.001$ by one-way ANOVA. **G,** Western blot for LLC cells treated with increasing concentrations of recombinant TNFα protein for GLUT1, HK2, or PGC-1α. β-Actin was used as the loading control. **H,** TNFα concentrations in the supernatant from LLC cultured with (+BMDM) or without (alone) BMDM, or in BMDM cultured with (+LLC) or without (alone) LLC, measured by ELISA. BD, below the detection limit. **, $P < 0.01$ by Student *t* test. **I,** Immunostaining of TNFα (red) and CD68 (green) in LLC tumors grown in mice. Nuclei are shown in blue with DAPI counterstaining. The inset shows magnified regions where indicated with the asterisk (*). White arrowheads, CD68-positive TAM-expressing TNFα. Scale bar, 100 μm. **J,** TNFα concentrations measured by ELISA in the supernatant from CD11b and F4/80 double-positive TAM sorted by FACS. Data are the mean ± SEM from triplicate determinations. ***, $P < 0.001$, determined by one-way ANOVA. **K,** TCGA analysis of clinical correlations between *CD68* and *TNF* (left) or between *TNF* and *HK2* (right) in 513 patients with adenocarcinoma NSCLC. *P* values are indicated in each plot.

Downloaded from http://aacrjournals.org/cancerres/article-pdf/79/4/795/2786616/795.pdf by guest on 15 September 2022

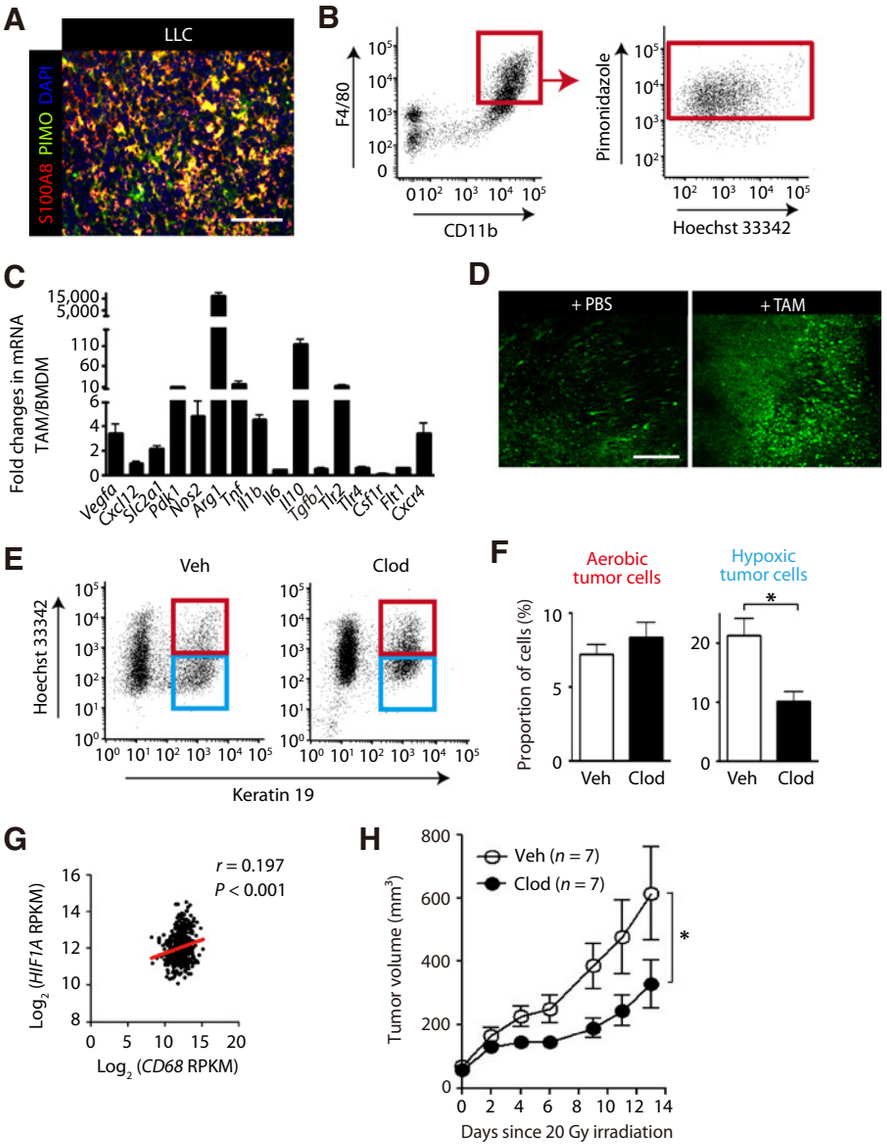

Figure 4.

TAMs directly contribute to tumor hypoxia. **A,** Immunostaining of LLC tumors grown in mice for TAM by using S100A8 (red) and hypoxia by using pimonidazole (PIMO; green) antibodies. Nuclei are shown in blue with DAPI counterstaining. **B,** FACS analysis demonstrating that CD11b and F4/80 double-positive TAMs are pimonidazole-positive. **C,** Gene expression in CD11b and F4/80 double-positive TAM isolated from LLC tumors compared with those in cultured BMDM. Data are the mean ± SEM from triplicate determinations. **D,** Two-photon microscopy images of the dorsal window chamber whereby 5 × HRE-GFP–expressing LLC tumors had been implanted. Images were taken at 24 hours after a single intratumoral injection of PBS (+PBS) or PBS containing FACS-sorted TAM (+TAM). Scale bars in **A** and **D**, 100 μm. **E,** Representative FACS plots demonstrating Hoechst^{bright}Keratin^{+} as aerobic tumor cells (red boxes) and Hoechst^{dim}Keratin^{+} as hypoxic tumor cells in LLC tumors grown in mice treated with Veh or Clod. **F,** Quantification of aerobic or hypoxic tumor cells in **E**. Data are the mean ± SEM for $n = 6$ mice per group. *, $P < 0.05$ by Student t test. **G,** TCGA analysis between *CD68* and *HIF1A* in 513 patients with adenocarcinoma NSCLC. P value is indicated in the graph. **H,** Growth of LLC tumor treated with Veh or Clod immediately prior to a single dose of 20 Gy ionizing irradiation. *, $P < 0.05$ by two-way ANOVA.

LLC cancer cells increased GLUT1 and HK2 protein expression (Fig. 3G) while decreasing peroxisome proliferator-activated receptor gamma coactivator 1-alpha (PGC-1α) expression (Fig. 3G) in a dose-dependent manner, suggesting that TNFα can facilitate glycolysis and inhibit mitochondrial biogenesis. To determine whether TNFα is mainly secreted from macrophages, we measured TNFα concentrations from the coculture system and found that TNFα was detectable in BMDM but not LLC (Fig. 3H) and more so when BMDM were cocultured with LLC (Fig. 3H). By examining LLC tumors grown in mice, we observed that TNFα was indeed expressed in CD68-expressing TAM (Fig. 3I) and that CD11b- and F4/80-double positive TAM sorted from these tumors secreted significant amount of TNFα into the medium (Fig. 3J). To further validate our preclinical results, we went back to TCGA database and found a strong correlation between *CD68* and *TNF* (Fig. 3K) and between *TNF* and *HK2* (Fig. 3K), indicating that TAMs produce TNFα and that this facilitates glycolysis in tumors.

TAMs exacerbate tumor hypoxia

We then wished to examine whether TAM could compete for oxygen with cancer cells thereby contributing to tumor hypoxia. To test our hypothesis, we first examined the distribution of TAM with respect to hypoxic regions in tumors by performing immunostaining of LLC tumors grown in mice for TAM and hypoxia using S100A8 antibodies and pimonidazole, respectively. We observed that numerous TAMs were positive for pimonidazole (Fig. 4A), indicating that TAM may be hypoxic. Immunophenotyping analysis further revealed that CD11b- and F4/80-double positive TAMs in LLC tumors were positive for pimonidazole (Fig. 4B). We then sorted CD11b- and F4/80-double positive TAM and analyzed the gene expression profile and found that TAM exhibited a significantly increased gene expression in the following pathways: hypoxic signaling including *Vegfa*, *Slc2a1*, *Pdk1*, and *C-X-C motif chemokine receptor-4* (*Cxcr4*); macrophage M1 polarization such as *Nos-2* as well as M2 polarization such as *arginase-1* (*Arg1*); and immunosuppressive cytokines such as *Tnf*

Downloaded from http://aacrjournals.org/cancerres/article-pdf/79/4/795/2786616/795.pdf by guest on 15 September 2022

and *Il10* compared with BMDM (Fig. 4C). Other genes known to be regulated by HIF including *Cxcl12* (26), *Il6* (30), *Tgfb1* (31), *toll-like receptor 4* (*Tlr4*; ref. 32), *Csf1r* (33), or *fms related tyrosine kinase 1* (*Flt1*; ref. 34) did not exhibit such an increase (Fig. 4C). To determine whether TAM can directly contribute to the tumor hypoxia, we sorted TAM by FACS as described above, labeled them with a cell tracker dye (Supplementary Fig. S3A), and injected them directly underneath a dorsal window chamber in nude mice, in which LLCs transfected with 5 times hypoxia-responsive element (5 × HRE)-GFP (35) were implanted. By two-photon microscopic imaging, we were able to observe that TAM injection significantly increased GFP signal in tumors (Fig. 4D), indicating that TAM can directly contribute to the tumor hypoxia.

To examine whether TAM depletion can alter the extent of tumor hypoxia, we administered Clod followed by Hoechst 33342 dye to LLC tumor–bearing mice and analyzed aerobic (Hoechst^{bright}Keratin^{+}) or hypoxic (Hoechst^{dim}Keratin^{+}) cancer cells (Fig. 4E). We found that Clod significantly decreased hypoxic tumor cell fractions (Fig. 4F), whereas aerobic cells were not affected (Fig. 4F). We observed similar results when we utilized pimonidazole in the place of Hoechst 33342 (Supplementary Fig. S3B). TCGA analyses further revealed that there was a significant correlation between *CD68* and *HIF1A* in 513 patients with adenocarcinoma NSCLC (Fig. 4G). Given that tumor hypoxia is a major resistance factor for radiotherapy (2), we examined whether the depletion of TAM could sensitize tumors to ionizing radiation. We found that only transient administration of Clod prior to ionizing radiation could result in a small but significant sensitization of LLC tumors to a single high dose of 20 Gy of irradiation (Fig. 4H). These results thus suggest that TAMs exacerbate tumor hypoxia.

AMP-activated protein kinase and PGC-1α activation in TAM promotes tumor hypoxia

To determine how TAMs contribute to tumor hypoxia, we first measured the oxygen consumption of BMDM or BMDM mixed with LLC in 1:5 or 1:10 ratio. We found that BMDM oxygen consumption rate became significantly slowed if they were mixed with cancer cells (Fig. 5A). Furthermore, ATP production was significantly decreased in BMDM if they were mixed with cancer cells at 1:5 or 1:10 ratio (Fig. 5B), indicating that BMDM competed oxygen with cancer cells. Exposure of cells to hypoxic

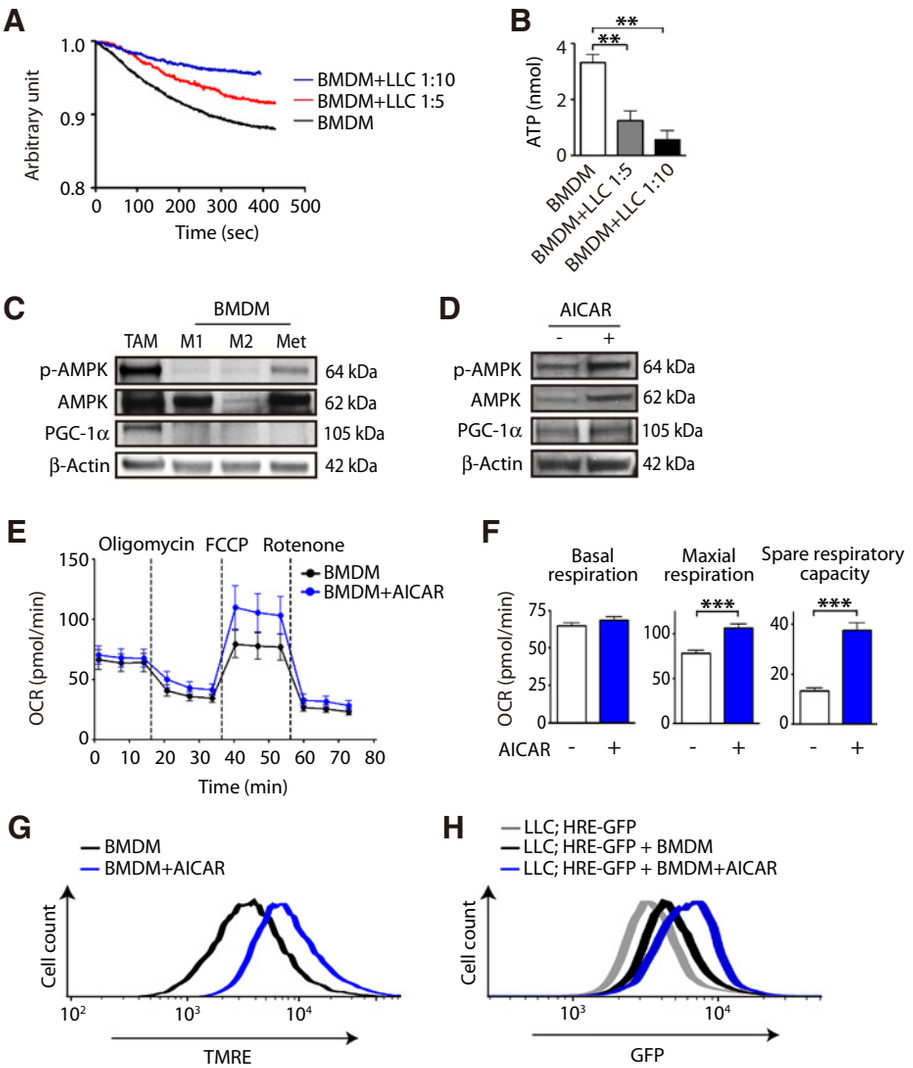

Figure 5.

AMPK and PCG-1α activation in TAM increases tumor hypoxia. **A,** Oxygen consumption kinetics in the BMDM alone (BMDM) or with LLC mixed in 1:5 (BMDM+LLC 1:5) or 1:10 (BMDM+LLC 1:10) ratio. **B,** ATP production from BMDM described in **A**. Data are the mean ± SEM from triplicate measurements. **, $P < 0.01$ by one-way ANOVA. **C,** Western blot for phospho-AMPK (p-AMPK), AMPK, or PGC-1α in FACS-sorted TAM, BMDM polarized to M1 or M2, or metformin (Met)-treated BMDM. **D,** Western blot of BMDM treated with or without AICAR. β-Actin was used as the loading control in **C** and **D**. **E** and **F,** Oxygen consumption rate (OCR; **E**) and its quantifications as basal respiration, maximal respiration, and spare respiratory capacity (**F**) in BMDM treated with or without AICAR. Data are the mean ± SEM for $n \geq 10$ replicates per group. ***, $P < 0.001$, determined by Student *t* test. **G,** FACS histogram demonstrating mitochondrial membrane potential in BMDM with or without AICAR, as measured by TMRE. **H,** FACS histogram demonstrating GFP signal intensity in LLC cells expressing 5 × HRE-GFP. These LLC cells were either cultured alone (LLC; HRE-GFP), cocultured with BMDM (LLC; HRE-GFP + BMDM), or cocultured with AICAR-treated BMDM (LLC; HRE-GFP + BMDM + AICAR).

Downloaded from http://aacrjournals.org/cancerres/article-pdf/79/4/795/2786616/795.pdf by guest on 15 September 2022

conditions may activate AMP-activated protein kinase (AMPK), a nutrient-sensing signaling pathway (36). To examine whether AMPK activation would be involved in TAM contributing to the tumor hypoxia, we sorted TAM from LLC tumor–bearing animals and examined phospho-AMPK levels by Western blot. We found that there was a strong expression of phospho-AMPK protein in TAM but not in M1- or M2-polarized BMDM (Fig. 5C). Furthermore, we observed a strong expression of PGC-1α, a master regulator for mitochondrial biogenesis activated by AMPK (37) in TAM (Fig. 5C), suggesting that the activation of AMPK therefore PGC-1α would lead to an increased mitochondrial biogenesis in TAM responsible for the oxygen consumption. To test this hypothesis, we used AICAR, a compound that can activate AMPK and PGC-1α (38) because metformin, an AMPK activator (39), failed to increase PGC-1α expression in BMDM (Fig. 5C). We observed that AICAR resulted in an increased expression of phospho-AMPK and PGC-1α in BMDM (Fig. 5D) as well as mitochondrial biogenesis including the increased oxygen consumption rate (Fig. 5E), maximal and spare respiration capacity (Fig. 5F), and mitochondrial membrane potential (Fig. 5G). We found that AICAR-treated BMDM when cocultured with LLC expressing 5 × HRE-GFP increased GFP signals compared with BMDM treated with vehicle (Fig. 5H). These results suggest that TAM may exacerbate tumor hypoxia by activated AMPK signaling.

TAMs dampen PD-L1 expression in tumors and inhibit T-cell infiltration

Tumor hypoxia and glycolysis have recently reported to inhibit cytotoxic T-cell functions (40, 41). Upon RNA sequencing analyses with the sorted aerobic cancer cells isolated from LLC treated with or without Clod, we found that the gene transcripts in defense response pathway were significantly downregulated in tumors depleted for TAM (Fig. 6A). To determine how TAMs affect the defense response, we analyzed tumor-infiltrating T cells in LLC grown in mice and observed that CD4 and CD8α T-cell infiltration was significantly increased in tumors depleted for TAM (Fig. 6B).

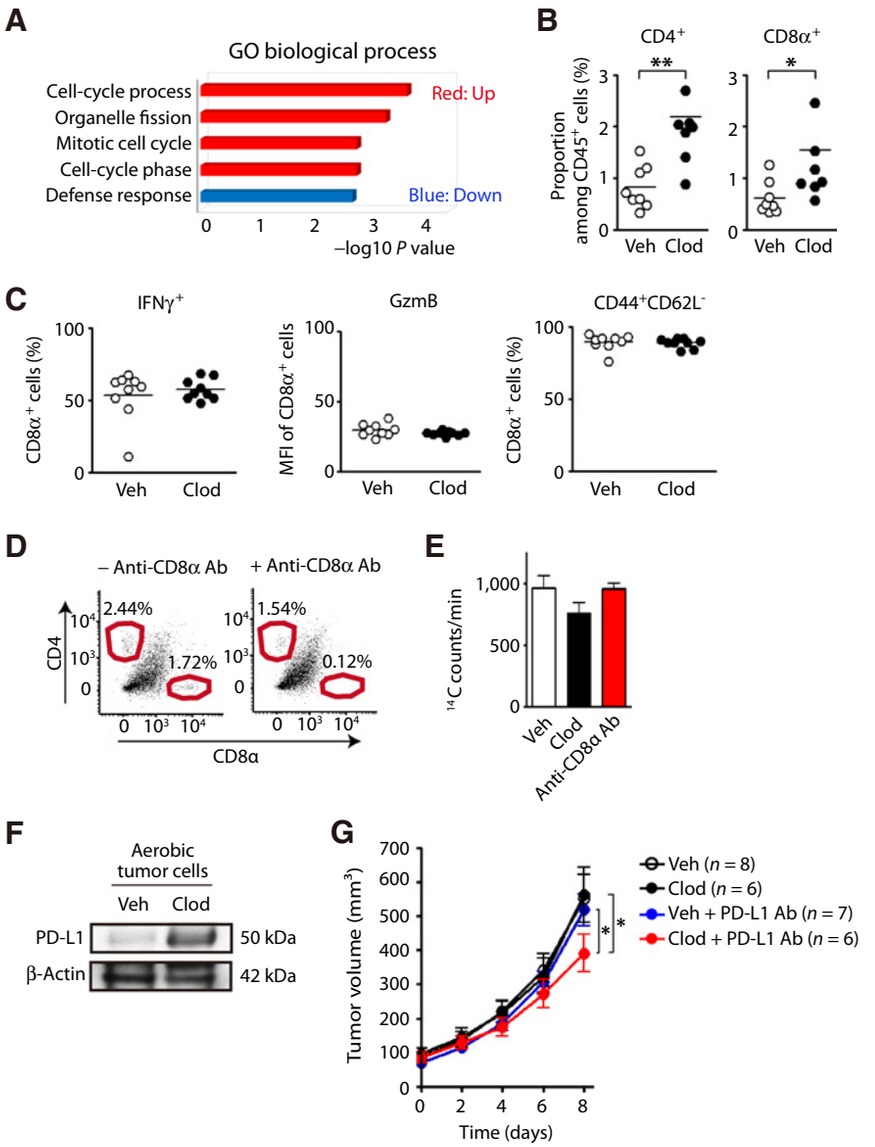

Figure 6.

Depletion of TAM increases tumor-infiltrating T cells and PD-L1 expression in tumors. **A,** Gene ontology (GO) biological process from RNA sequencing analyses in FACS-sorted aerobic cancer cells isolated from LLC tumors treated with Clod or Veh. **B,** FACS analysis of the number of $CD4^+$ or $CD8\alpha^+$ tumor-infiltrating T cells in LLC tumors treated with Veh ($n = 8$) or Clod ($n = 7$). *, $P < 0.05$; **, $P < 0.01$, by Student t test. **C,** FACS analysis for $IFN\gamma^+$, GzmB, or $CD44^+CD62L^-$ cells among $CD8\alpha^+$ T cells in LLC tumors treated with Veh ($n = 9$) or Clod ($n = 9$). GzmB is presented by mean fluorescence intensity (MFI). **D,** Representative FACS plots for $CD4^+$ or $CD8\alpha^+$ T cells (red boxes) in LLC tumors treated with (+anti-CD8α Ab) or without (-anti-CD8α Ab) anti-CD8α antibodies (Ab). Percentages are $CD4^+$ or $CD8\alpha^+$ T cells among the total $CD45^+$ lymphocytes in tumors. **E,** Glucose uptake in the sorted aerobic cancer cells isolated from LLC treated with Veh, Clod, or anti-CD8α Ab. Data are the mean ± SEM from at least triplicate samples per group. **F,** Western blot for PD-L1 expression in FACS-sorted aerobic cancer cells isolated from tumors treated with Veh or Clod. β-Actin was used as the loading control. **G,** LLC tumor growth in mice treated with Veh, Clod, Veh + PD-L1 Ab, or Clod + PD-L1 Ab. Data are the mean ± SEM with number of animals indicated in the graphs. *, $P < 0.05$ by two-way ANOVA.

Downloaded from http://aacrjournals.org/cancerres/article-pdf/79/4/795/2786616/795.pdf by guest on 15 September 2022

Further analyses revealed that Clod treatment did not affect IFNγ, GzmB, or CD62L expression in CD8α T cells (Fig. 6C), indicating that TAM may inhibit T-cell infiltration to tumors but not activation. To examine whether the increased T-cell infiltration may increase tumor glycolysis similarly as to TAM, we administered anti–CD8α-neutralizing antibodies to tumor-bearing mice and examined glucose uptake (Fig. 6D). We found that depletion of CD8α T cells did not change glucose uptake into aerobic cancer cells (Fig. 6E). We next examined PD-L1 expression in aerobic cancer cells isolated from tumors depleted for TAM. We found that aerobic cancer cells depleted for TAM exhibited a significantly increased PD-L1 expression (Fig. 6F), and this may be caused by increased T-cell infiltration to tumors as T-cell–secreted IFNγ is known to induce PD-L1 expression in cancer cells (42). These results suggest TAM depletion could sensitize tumors to PD-L1 blockade, and we indeed observed that anti–PD-L1 antibodies were effective in reducing the tumor growth only when combined with TAM depletion by Clod (Fig. 6G).

Discussion

Clinically, it has been recognized for some time that the presence of inflammation confounds FDG-positive signals in PET images of patients with cancer (43). Recently, Lee and colleagues (44) have demonstrated that depletion of macrophages by Clod resulted in a significant reduction of FDG signals in the heart following acute myocardial infarction in mice, indicating that macrophages can take up significant amount of glucose, well supporting our results present in this study. In this study, we found that TAM can contribute to tumor hypoxia and glycolysis. Previous studies have demonstrated that TAMs migrate toward hypoxic areas of tumors, and their motility slows once trapped in those regions via semaphorin 3A acting as a stop signal (14). In our study, we found that TAMs were hypoxic themselves (Fig. 4B) and exhibited a strong expression of phospho-AMPK (Fig. 5C). AMPK activation in cells has been suggested to skew their cell metabolism toward oxidative phosphorylation (45), consistent with our results demonstrating that AMPK activation in BMDM leads to an increased oxygen consumption ratio and mitochondrial membrane potential (Fig. 5E–G). We also found in our study that macrophage-secreted TNFα resulted in an increase in glycolysis in cancer cells (Fig. 3F). TNFα can be produced from macrophages by activation of TLR4, leading to NF-κB signaling pathways (46) and that various danger-associated molecular pattern molecules, including heat shock proteins, and high-mobility group box-1 secreted from apoptotic or necrotic tumor cells can activate TLR4 on macrophages (47).

TAMs are extensively documented for their roles in inhibiting antitumor cytotoxic T-cell responses for example by secreting immunosuppressive cytokines such as TGFβ (48). Recently, recent imaging study (49) has elegantly demonstrated that TAMs hijack PD-1 antibodies that had been initially bound to cytotoxic T cells hence abrogating its antitumor efficacy. Chang and colleagues (40) have further suggested that tumor glycolysis can restrict T-cell activation necessary for antitumor immune responses. We have demonstrated that depletion of TAM makes tumors less hypoxic and glycolytic and that this may have resulted in an increased T-cell infiltration, leading to an increased PD-L1 expression in tumors (Fig. 6). The latter has a tremendously important clinical implication because patients' eligibility criteria PD-L1 blockade therapies are based on PD-L1 expression in their tumor biopsy samples (50). Our results thus demonstrate that TAM can modulate tumor metabolism as well as PD-L1 expression in tumors, compromising the tumor response to various anticancer therapies, including the latest immunotherapy.

Disclosure of Potential Conflicts of Interest

J.S. Lee is CEO at Brightonix Imaging Inc. I.L. Weissman is co-founder, director at, and is a consultant/advisory board member for Forty Seven Inc. No potential conflicts of interest were disclosed by the other authors.

Authors' Contributions

Conception and design: H. Jeong, B.-J. Hong, P. Tessier, M. Pelletier, J.H. Ju, S. Kim, I.H. Kim, H.J. Kim, J.-W. Park, G.J. Cheon, Y.K. Jeon, G.-O. Ahn

Development of methodology: H. Jeong, B.-J. Hong, C.-J. Lee, M.S. Lee, S. Kim, J.S. Lee, G.J. Cheon

Acquisition of data (provided animals, acquired and managed patients, provided facilities, etc.): H. Jeong, S. Kim, Y.-E. Kim, S. Bok, J.-M. Oh, S.-H. Gwak, M.Y. Yoo, M.S. Lee, S.-J. Chung, J. Defrêne, H. Jeon, T.-Y. Roh, B. Kim, K.H. Kim, J.H. Ju, Y.-J. Lee, H.J. Kim, J.S. Lee, G.J. Cheon, D.H. Chung, Y.K. Jeon, G.-O. Ahn

Analysis and interpretation of data (e.g., statistical analysis, biostatistics, computational analysis): H. Jeong, S. Kim, B.-J. Hong, C.-J. Lee, Y.-E. Kim, S. Bok, J.-M. Oh, S.-H. Gwak, M.S. Lee, J. Defrêne, P. Tessier, M. Pelletier, H. Jeon, T.-Y. Roh, B. Kim, K.H. Kim, J.H. Ju, D.-W. Kim, I.H. Kim, H.J. Kim, G.J. Cheon, I.L. Weissman, Y.K. Jeon, G.-O. Ahn

Writing, review, and/or revision of the manuscript: H. Jeong, D.-W. Kim, G.J. Cheon, I.L. Weissman, Y.K. Jeon, G.-O. Ahn

Administrative, technical, or material support (i.e., reporting or organizing data, constructing databases): B.-J. Hong, C.-J. Lee, S.-J. Chung, J.H. Ju, H.J. Kim, J.-W. Park, G.J. Cheon, Y.K. Jeon, G.-O. Ahn

Study supervision: G.J. Cheon, Y.K. Jeon, G.-O. Ahn

Acknowledgments

We would like to thank Dr. J. Martin Brown (Stanford University) for LLC cell line and 5 × HRE-GFP construct, Drs. Mark Dewhirst and Gregory Palmer (Duke University) for sharing *in vivo* dorsal window chamber techniques, and Drs. Andrew Minchinton and Kevin Bennewith (British Columbia Cancer Research Centre) for *in vivo* Hoechst 33342 FACS protocol. We are grateful to Kook-Chan Heo at GENIA Inc. and Sang-Kwon Lee at Hana BioTech for arranging animal housing and transportation between POSTECH and Seoul National University College of Medicine. Geun Bae Ko and Kyeong Yun Kim at the Department of Nuclear Medicine, Seoul National University College of Medicine, are also acknowledged for their contributions for developing the small animal PET/MRI instrument used in this study. We also appreciate help from Narae Park (Seoul St. Mary's Hospital) for reagents, Ji Yong Park (the Department of Nuclear Medicine, Seoul National University College of Medicine) with ferumoxytol preparation and technical information, A-Ram Kim (KIRAM) for a mouse lung cancer model, and Hyung-Seok Choi (POSTECH) for sharing a protocol analyzing T cells in tumors. Special thanks go to the staffs at the FACS core and animal facility at POSTECH for their technical and maintenance support; staffs at the Department of Pathology at Seoul National University College of Medicine for handling and preparing patients' specimen. This work was supported by grants from the National R&D Program for Cancer Control, the Ministry of Health and Welfare (1320220 to G.-O. Ahn); the Ministry of Science, ICT, and Future Planning Korea (grant numbers NRF-2017M2A2A7A01015968 and NRF-2018R1A2B6004453 to G.-O. Ahn; NRF-2017M2A2A7A01070925 to H.J. Kim); 4th Green Science grant from Pohang Steel Company (POSCO) to G.-O. Ahn; Ludwig Cancer Foundation to I.L. Weissman; and BK21 Plus program from the Ministry of Education Korea (Grant No. 10Z20130012243). B.-J. Hong (NRF-2013H1A2A1032808) and Y.-E. Kim (NRF-2012H1A2A1002871) are Global PhD fellows supported by the Ministry of Science, ICT, and Future Planning Korea; H. Jeong is a recipient of TJ Park CheongAm POSCO Science Fellowship.

The costs of publication of this article were defrayed in part by the payment of page charges. This article must therefore be hereby marked *advertisement* in accordance with 18 U.S.C. Section 1734 solely to indicate this fact.

Received August 15, 2018; revised December 3, 2018; accepted December 27, 2018; published first January 4, 2019.

Downloaded from http://aacrjournals.org/cancerres/article-pdf/79/4/795/2786616/795.pdf by guest on 15 September 2022

References

1. Kroemer G, Pouyssegur J. Tumor cell metabolism: cancer's Achilles' heel. Cancer Cell 2008;13:472–82.
2. Brown JM, Wilson WR. Exploiting tumour hypoxia in cancer treatment. Nat Rev Cancer 2004;4:437–47.
3. Brizel DM, Scully SP, Harrelson JM, Layfield LJ, Bean JM, Prosnitz LR, et al. Tumor oxygenation predicts for the likelihood of distant metastases in human soft tissue sarcoma. Cancer Res 1996;56:941–3.
4. Noman MZ, Buart S, Van Pelt J, Richon C, Hasmim M, Leleu N, et al. The cooperative induction of hypoxia-inducible factor-1 alpha and STAT3 during hypoxia induced an impairment of tumor susceptibility to CTL-mediated cell lysis. J Immunol 2009;182:3510–21.
5. Warburg O. On the origin of cancer cells. Science 1956;123:309–14.
6. Rohren EM, Turkington TG, Coleman RE. Clinical applications of PET in oncology. Radiology 2004;231:305–32.
7. Stine ZE, Walton ZE, Altman BJ, Hsieh AL, Dang CV. MYC, metabolism, and cancer. Cancer Discov 2015;5:1024–39.
8. Suzuki H, Nishio M, Nakanishi H, Hanai N, Hirakawa H, Kodaira T, et al. Impact of total lesion glycolysis measured by (18)F-FDG-PET/CT on overall survival and distant metastasis in hypopharyngeal cancer. Oncol Lett 2016;12:1493–500.
9. Bhatt AN, Chauhan A, Khanna S, Rai Y, Singh S, Soni R, et al. Transient elevation of glycolysis confers radio-resistance by facilitating DNA repair in cells. BMC Cancer 2015;15:335.
10. Sonveaux P, Vegran F, Schroeder T, Wergin MC, Verrax J, Rabbani ZN, et al. Targeting lactate-fueled respiration selectively kills hypoxic tumor cells in mice. J Clin Invest 2008;118:3930–42.
11. Noy R, Pollard JW. Tumor-associated macrophages: from mechanisms to therapy. Immunity 2014;41:49–61.
12. Liu SC, Alomran R, Chernikova SB, Lartey F, Stafford J, Jang T, et al. Blockade of SDF-1 after irradiation inhibits tumor recurrences of autochthonous brain tumors in rats. Neuro Oncol 2014;16:21–8.
13. Du R, Lu KV, Petritsch C, Liu P, Ganss R, Passegue E, et al. HIF1alpha induces the recruitment of bone marrow-derived vascular modulatory cells to regulate tumor angiogenesis and invasion. Cancer Cell 2008;13:206–20.
14. Casazza A, Laoui D, Wenes M, Rizzolio S, Bassani N, Mambretti M, et al. Impeding macrophage entry into hypoxic tumor areas by Sema3A/Nrp1 signaling blockade inhibits angiogenesis and restores antitumor immunity. Cancer Cell 2013;24:695–709.
15. Wang H, Shao Q, Sun J, Ma C, Gao W, Wang Q, et al. Interactions between colon cancer cells and tumor-infiltrated macrophages depending on cancer cell-derived colony stimulating factor 1. Oncoimmunology 2016;5:e1122157.
16. Pollard JW. Tumour-educated macrophages promote tumour progression and metastasis. Nat Rev Cancer 2004;4:71–8.
17. Galvan-Pena S, O'Neill LA. Metabolic reprograming in macrophage polarization. Front Immunol 2014;5:420.
18. De Palma M, Murdoch C, Venneri MA, Naldini L, Lewis CE. Tie2-expressing monocytes: regulation of tumor angiogenesis and therapeutic implications. Trends Immunol 2007;28:519–24.
19. Gordon SR, Maute RL, Dulken BW, Hutter G, George BM, McCracken MN, et al. PD-1 expression by tumour-associated macrophages inhibits phagocytosis and tumour immunity. Nature 2017;545:495–9.
20. Nywening TM, Belt BA, Cullinan DR, Panni RZ, Han BJ, Sanford DE, et al. Targeting both tumour-associated CXCR2(+) neutrophils and CCR2(+) macrophages disrupts myeloid recruitment and improves chemotherapeutic responses in pancreatic ductal adenocarcinoma. Gut 2018;67:1112–23.
21. Ahn GO, Tseng D, Liao CH, Dorie MJ, Czechowicz A, Brown JM. Inhibition of Mac-1 (CD11b/CD18) enhances tumor response to radiation by reducing myeloid cell recruitment. Proc Natl Acad Sci U S A 2010;107:8363–8.
22. Goodwin J, Neugent ML, Lee SY, Choe JH, Choi H, Jenkins DMR, et al. The distinct metabolic phenotype of lung squamous cell carcinoma defines selective vulnerability to glycolytic inhibition. Nat Commun 2017;8:15503.
23. van Rooijen N, Sanders A, van den Berg TK. Apoptosis of macrophages induced by liposome-mediated intracellular delivery of clodronate and propamidine. J Immunol Methods 1996;193:93–9.
24. Daldrup-Link HE, Golovko D, Ruffell B, Denardo DG, Castaneda R, Ansari C, et al. MRI of tumor-associated macrophages with clinically applicable iron oxide nanoparticles. Clin Cancer Res 2011;17:5695–704.
25. Bennewith KL, Durand RE. Quantifying transient hypoxia in human tumor xenografts by flow cytometry. Cancer Res 2004;64:6183–9.
26. Hitchon C, Wong K, Ma G, Reed J, Lyttle D, El-Gabalawy H. Hypoxia-induced production of stromal cell-derived factor 1 (CXCL12) and vascular endothelial growth factor by synovial fibroblasts. Arthritis Rheum 2002;46:2587–97.
27. Wheaton WW, Weinberg SE, Hamanaka RB, Soberanes S, Sullivan LB, Anso E, et al. Metformin inhibits mitochondrial complex I of cancer cells to reduce tumorigenesis. Elife 2014;3:e02242.
28. Huang CC, Wang SY, Lin LL, Wang PW, Chen TY, Hsu WM, et al. Glycolytic inhibitor 2-deoxyglucose simultaneously targets cancer and endothelial cells to suppress neuroblastoma growth in mice. Dis Model Mech 2015;8:1247–54.
29. Hao W, Chang CP, Tsao CC, Xu J. Oligomycin-induced bioenergetic adaptation in cancer cells with heterogeneous bioenergetic organization. J Biol Chem 2010;285:12647–54.
30. Jeong HJ, Hong SH, Park RK, Shin T, An NH, Kim HM. Hypoxia-induced IL-6 production is associated with activation of MAP kinase, HIF-1, and NF-kappaB on HEI-OC1 cells. Hear Res 2005;207:59–67.
31. Deng B, Zhu JM, Wang Y, Liu TT, Ding YB, Xiao WM, et al. Intratumor hypoxia promotes immune tolerance by inducing regulatory T cells via TGF-beta1 in gastric cancer. PLoS One 2013;8:e63777.
32. Kim SY, Choi YJ, Joung SM, Lee BH, Jung YS, Lee JY. Hypoxic stress up-regulates the expression of Toll-like receptor 4 in macrophages via hypoxia-inducible factor. Immunology 2010;129:516–24.
33. Chaturvedi P, Gilkes DM, Takano N, Semenza GL. Hypoxia-inducible factor-dependent signaling between triple-negative breast cancer cells and mesenchymal stem cells promotes macrophage recruitment. Proc Natl Acad Sci U S A 2014;111:E2120–9.
34. Okuyama H, Krishnamachary B, Zhou YF, Nagasawa H, Bosch-Marce M, Semenza GL. Expression of vascular endothelial growth factor receptor 1 in bone marrow-derived mesenchymal cells is dependent on hypoxia-inducible factor 1. J Biol Chem 2006;281:15554–63.
35. Shibata T, Giaccia AJ, Brown JM. Development of a hypoxia-responsive vector for tumor-specific gene therapy. Gene Ther 2000;7:493–8.
36. Marsin AS, Bouzin C, Bertrand L, Hue L. The stimulation of glycolysis by hypoxia in activated monocytes is mediated by AMP-activated protein kinase and inducible 6-phosphofructo-2-kinase. J Biol Chem 2002;277:30778–83.
37. Jager S, Handschin C, St-Pierre J, Spiegelman BM. AMP-activated protein kinase (AMPK) action in skeletal muscle via direct phosphorylation of PGC-1alpha. Proc Natl Acad Sci U S A 2007;104:12017–22.
38. Irrcher I, Adhihetty PJ, Sheehan T, Joseph AM, Hood DA. PPARgamma coactivator-1alpha expression during thyroid hormone- and contractile activity-induced mitochondrial adaptations. Am J Physiol Cell Physiol 2003;284:C1669–77.
39. Kim J, Yang G, Kim Y, Kim J, Ha J. AMPK activators: mechanisms of action and physiological activities. Exp Mol Med 2016;48:e224.
40. Chang CH, Qiu J, O'Sullivan D, Buck MD, Noguchi T, Curtis JD, et al. Metabolic competition in the tumor microenvironment is a driver of cancer progression. Cell 2015;162:1229–41.
41. Westendorf AM, Skibbe K, Adamczyk A, Buer J, Geffers R, Hansen W, et al. Hypoxia enhances immunosuppression by inhibiting CD4+ Effector T cell function and promoting treg activity. Cell Physiol Biochem 2017;41:1271–84.
42. Garcia-Diaz A, Shin DS, Moreno BH, Saco J, Escuin-Ordinas H, Rodriguez GA, et al. Interferon receptor signaling pathways regulating PD-L1 and PD-L2 Expression. Cell Rep 2017;19:1189–201.
43. Strauss LG. Fluorine-18 deoxyglucose and false-positive results: a major problem in the diagnostics of oncological patients. Eur J Nucl Med 1996;23:1409–15.
44. Lee WW, Marinelli B, van der Laan AM, Sena BF, Gorbatov R, Leuschner F, et al. PET/MRI of inflammation in myocardial infarction. J Am Coll Cardiol 2012;59:153–63.
45. Biswas SK. Metabolic reprogramming of immune cells in cancer progression. Immunity 2015;43:435–49.

Downloaded from http://aacrjournals.org/cancerres/article-pdf/79/4/795/2786616/795.pdf by guest on 15 September 2022

46. Palsson-McDermott EM, O'Neill LA. Signal transduction by the lipopolysaccharide receptor, Toll-like receptor-4. Immunology 2004;113:153–62.
47. Schaefer L. Complexity of danger: the diverse nature of damage-associated molecular patterns. J Biol Chem 2014;289:35237–45.
48. Doedens AL, Stockmann C, Rubinstein MP, Liao D, Zhang N, DeNardo DG, et al. Macrophage expression of hypoxia-inducible factor-1 alpha suppresses T-cell function and promotes tumor progression. Cancer Res 2010;70:7465–75.
49. Arlauckas SP, Garris CS, Kohler RH, Kitaoka M, Cuccarese MF, Yang KS, et al. In vivo imaging reveals a tumor-associated macrophage-mediated resistance pathway in anti-PD-1 therapy. Sci Transl Med 2017;9.
50. Mathew M, Safyan RA, Shu CA. PD-L1 as a biomarker in NSCLC: challenges and future directions. Ann Transl Med 2017;5:375.

Downloaded from http://aacrjournals.org/cancerres/article-pdf/79/4/795/2786616/795.pdf by guest on 15 September 2022